Stratigraphic architecture and petrophysical characterization of formations for deep disposal in the Fort Worth Basin, Texas

Katie M. Smye[1], Casee R. Lemons[1], Ray Eastwood[1], Guinevere McDaid[1], and Peter H. Hennings[1]

Abstract

Disposal of hydraulic fracturing flowback and produced water into Ordovician and Cambrian formations of the Fort Worth Basin (FWB), coupled with an increase in observed seismicity in the Dallas-Fort Worth area, necessitates an understanding of the geologic character of these disposal targets. More than 2 billion barrels (Bbbls) of wastewater have been disposed into the Ordovician Ellenburger Group of the FWB over the past 35 years. Since the implementation of the TexNet Earthquake Catalog (1 January 2017), more than 20 earthquakes of local magnitude ML2.0 or greater have been detected in the area, with depths ranging from 2 to 10 km (approximately 6500–33,000 ft). The cited mechanism for inducement of these earthquakes is reactivation of basement faults due to pore pressure changes, either directly related to proximal disposal or due to disposal volume buildup over time. Here, we present a stratigraphic and petrophysical analysis of FWB disposal targets and their relation to basement rocks. The Ellenburger consists of alternating layers of limestone and dolomite, with minor siliciclastics above the basement toward the Llano Uplift. Matrix porosity averages <5 porosity units (p.u.), with higher porosity in dolomitic layers than in limestone. Dolomite dominates at the top of the Ellenburger, which was exposed at the end of both the Lower and Upper Ordovician. Where crystalline basement rocks are penetrated, the composition ranges from granitic to chlorite-bearing metamorphosed lithology. The basement-sediment interface is frequently marked by increased porosity. An updated map of structure on top of basement indicates elevations ranging from outcrop at the Llano Uplift to more than −12,200 ft (−3.7 km) subsea toward the northeast. The disposal zone pore volume is estimated from thickness and porosity maps and ranges from <0.1 to >0.60 billion barrels per square mile (Bbbl/mi^2).

Introduction

In the Fort Worth Basin (FWB), Texas, flowback and produced water associated with Barnett Shale gas production is disposed into the underlying Ellenburger Group and has been linked to increased seismic activity since 2008 (Frohlich, 2012; Hornbach et al., 2015, 2016; Frohlich et al., 2016; Scales et al., 2017). The mechanism linking disposal and induced seismicity is based on the hydraulic connectivity of an overpressured disposal formation and the seismogenic basement (e.g., Zhang et al., 2013; Frohlich et al., 2014; Hornbach et al., 2015; Walsh and Zoback, 2015; Scales et al., 2017; Hincks et al., 2018).

From 2000 to 2017, more than 2 Bbbls of saltwater have been disposed into the locally unproductive Cambrian-Ordovician-aged formations of the FWB, including the Ellenburger Group, via 166 disposal wells (Figure 1a). These formations are the primary disposal targets, with increased disposal volumes after 2008 (Figure 1b), spatially and temporally coincident with Barnett Shale production. Disposal well completion methods are plug and perf (50%), openhole (48%), and existing open-hole zones with new perforations (2%); Cambrian-Ordovician disposal depths range from Viola-Simpson to near the top of the basement.

The stratigraphic architecture and rock properties of the disposal intervals, and their relation to basement rocks, are key in understanding the disposal reservoir, the flow of injected fluid, and the potential for induced seismicity (e.g., National Research Council, 2013; Zhang et al., 2013; Shah and Keller, 2017; Hincks et al., 2018). This type of geologic analysis is integral to any attempt to model not only historical disposal and induced seismicity but also to predict areas of concern based on potential pore pressure increases and reactivation of basement faults.

Several outcrop studies have been undertaken on the Ordovician Ellenburger Group and Cambrian Moore Hollow Group near the Llano Uplift (e.g., Cloud et al., 1945; Crowley and Hendricks, 1945; Cloud and Barnes,

[1]University of Texas at Austin, Bureau of Economic Geology, Austin, Texas, USA. E-mail: katie.smye@beg.utexas.edu (corresponding author); casee.lemons@beg.utexas.edu; ray.eastwood@beg.utexas.edu; guin.mcdaid@beg.utexas.edu; peter.hennings@beg.utexas.edu.

Manuscript received by the Editor 26 October 2018; revised manuscript received 11 February 2019; published ahead of production 06 August 2019; published online 15 October 2019. This paper appears in *Interpretation*, Vol. 7, No. 4 (November 2019); p. SL1–SL17, 13 FIGS., 1 TABLE.
http://dx.doi.org/10.1190/INT-2018-0195.1.

1948; Hendricks, 1952; Barnes et al., 1959; Barnes and Bell, 1977; synthesized in Wright, 1962, 1979; Bradfield, 1964; Hendricks, 1964; Watson, 1980; Collier, 1983), with limited attempts to correlate formations in the subsurface based on physical properties. Similarly, subdivision and correlation of units within the Ellenburger of the Delaware and Val Verde Basins has proven difficult (Ijirigho, 1981).

This paper contains a geologic characterization of Ordovician and Cambrian formations used for fluid disposal in the FWB, as well as an understanding of the basement-sediment interface and depth-to-basement. Interpretations are based on stratigraphic and petrophysical analyses of wireline well logs. We show that the Ellenburger of the FWB consists of alternating layers of limestone and dolomite, with minor porous siliciclastics at the base of the section toward the Llano Uplift. Due to uplift and erosion, the uppermost Ellenburger is only observed in the subsurface of the FWB and has a high dolomite fraction with increased porosity. The sediment-basement interface contains granite wash in some wells; elsewhere, carbonates directly overlie basement rocks. The lithology of the basement ranges from granitic to metamorphic composition.

These findings provide an understanding of the geology of the disposal formations in the FWB, including their stratigraphic architecture and petrophysical properties. The characterization of properties that influence flow, such as porosity, and their facies associations, lateral continuity, and geometry, provides needed geologic context for the flow of injected fluid and the potential for induced seismicity.

Geologic background

The FWB is an asymmetric, north–south elongated basin bounded by structural features of the Ouachita thrust front to the east, Muenster and Red River arches to the north, the Llano Uplift to the south, and the Bend Arch to the west. It is one of several foreland basins, including the Appalachian, Val Verde, and Anadarko, which formed during the Paleozoic in front of the Ouachita-Allegheny-Marathon Foldbelt. The basin contains up to 12,000 ft (3.6 km) of preserved sediment fill (Walper, 1982; Montgomery et al., 2005), including the Mississippian-age Barnett Shale, which has been widely targeted for natural gas production.

Most of the basement of the FWB is part of the Texas Craton, consisting of plutons — predominantly granite and diorite — emplaced into metasedimentary hornblende and biotite-schist, gneiss, and marble. Plutonic rocks make up most of the Texas Craton, with metasedimentary rocks of secondary importance (Flawn, 1956). In the subsurface, basement lithology has been interpreted through gravimetric anomalies (e.g., Olorunsola et al., 2015). The Abilene Gravity Minimum in the western FWB has been interpreted to reflect a granitic batholith 4–16 km (approximately 13,000–20,000 ft) thick that probably represents a Middle Proterozoic continental margin arc batholith, such as the Sierra Nevada, with an age of 1.4–1.34 Ga (Adams and Keller, 1996).

The Precambrian basement surface was exposed and eroded for more than 500 million years (Clabaugh and McGehee, 1962), and exhibited local relief of up to 800 ft (240 m) (Barnes and Bell, 1977). Initiation of a Wilson Cycle — opening and subsequent closing of

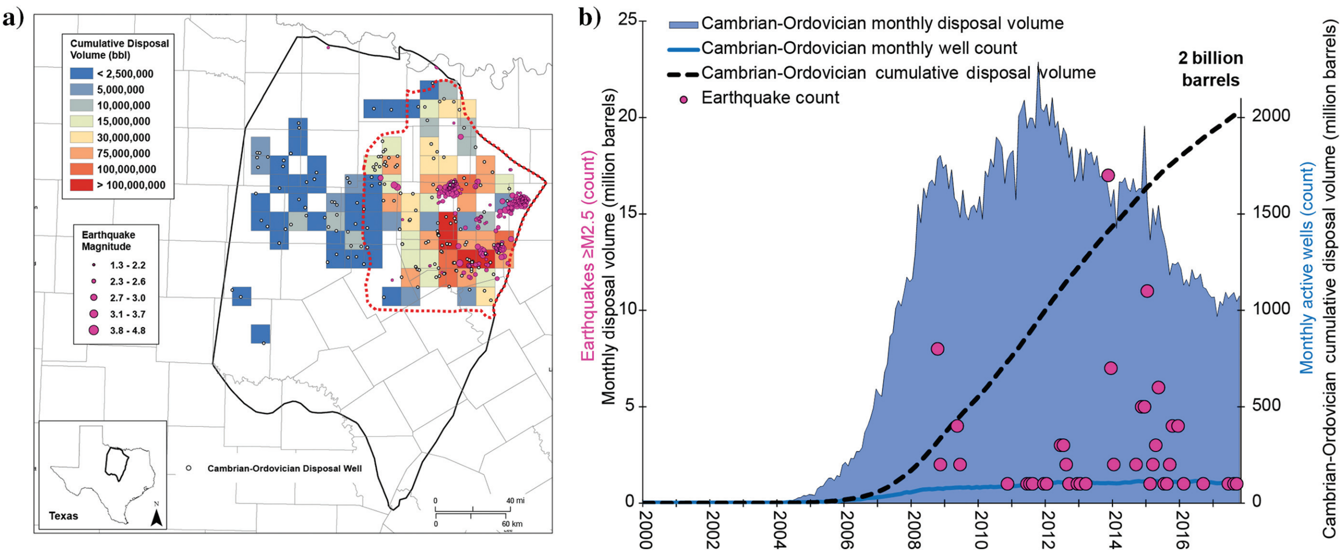

Figure 1. (a) Distribution of Cambrian-Ordovician saltwater disposal (SWD) wells (white dots) within the core Barnett producing area (dashed red line) and greater FWB study area (black line), along with cumulative Cambrian-Ordovician SWD volumes for each 100 mi^2 area and earthquake locations (pink dots). (b) Distribution of SWD volume and monthly count of active wells with and earthquake activity (pink dots). Earthquakes were identified by combining the SMU Earthquake Catalog (Quinones et al., 2019) and the USGS Earthquake Catalog (USGS, 2018).

an oceanic basin — led to formation of the proto-Atlantic (Iapetus) Ocean in this region. The ancestral divergent plate margin is evidenced by the Delaware, Southern Oklahoma, and Reelfoot Aulacogens (Walper, 1977; Adams and Keller, 1996). Deposition of siliciclastics, shelf facies (carbonates), and deeper Ouachita basinal facies occurred throughout the Late Cambrian and Early Ordovician (Figure 2).

The extent of siliciclastic deposition during Cambrian sea transgression is unclear, with some studies (e.g., Barnes et al., 1959) suggesting that the Hickory — the basal member of the Riley Formation (Figure 3) — laps out northeast of the Llano uplift, and other studies (e.g., Bradfield, 1964) hypothesizing that it extends into the FWB. Barnes and Bell (1977) suggest pinchout of sandstones away from the Llano Uplift, with the zero thickness line extending from Shackleford to Eastland and Erath Counties. Local thickness variations are related to Precambrian basement topography.

Although Cambrian siliciclastics are dominantly quartz sand (Cornish, 1975; Krause, 1996; McBride et al., 2002), feldspar is locally important based on proximity to buried granite hills (Barnes and Bell, 1977). Sediments of the Hickory appear to have been transported from north–northwest to south–southeast (Alsalem et al., 2017). Detrital zircon ages (1.451–1.325 Ga) indicate that the grains were derived from the granite-rhyolite province and transported by paleorivers draining the Texas Arch, a structural high on the flank of the transcontinental arch (Figure 2).

Other calcareous sandstones deposited during the Cambrian grade laterally and vertically into the Hickory where intervening limestone is absent. In the subsurface northwest of Llano, Cambrian sands have been interpreted as either Hickory (Barnes et al., 1959) or stratigraphically higher, possibly Lion Mountain equivalent (Figure 3) (Cornish, 1975). Limestones of the Upper Cambrian are generally more granular, glauconitic, and darker in color than those of the Ellenburger, and the dolomites are finer grained. Facies shifts are observed (Cloud and Barnes, 1948), and thickness variations are attributed to the local depositional rate and temporary nondeposition.

The Ordovician Ellenburger Group has been divided into the Tanyard, Gorman, and Honeycut Formations in outcrop (Figure 3). Limestone and dolomite are common, in contrast to the Ellenburger of the Permian Basin that is extensively dolomitized (Loucks and Kerans, 2019). Abrupt lateral transitions from calcitic to dolomitic facies have been attributed to lateral facies changes, collapse contacts, or faults. Limestone in outcrop frequently gives way to dolomite in the subsurface toward the east. Scattered sand — though not sand beds — is present in the Gorman and lower Honeycut Formations.

Cratonic unrest of the Ordovician, possibly related to the closing of the marginal basin and subduction of marginal basin crust beneath the volcanic arc in the Appalachian region, i.e., the Taconic Orogeny (Hiscott, 1978; Cooke et al., 1979; Walper, 1982), led to upwarping trending north–northwest from the Llano region (Turner, 1957; Walper, 1982). Carbonate shelf — and possibly slope — facies, including the Ellenburger Group, were regionally exposed. Any significant Late Ordovician, Silurian, Devonian, and Early Mississippian deposits were eroded, although remnants can be found as karst fill in the Llano region. Erosion in the FWB area was greatest toward the southwest. The Honeycut Formation present in outcrop disappears by westward truncation and "post-Honeycut" beds — i.e., those younger than any Honeycut observed in outcrop or core — are surmised to exist in the deeper FWB to the east. In the Permian Basin, up to seven unconformities have been identified due to periods of exposure (Combs et al., 2003). Whether these intermittent periods of exposure also occurred during the Ordovician in the FWB has not been determined.

Methodology

The study area is delineated by areas of intense Barnett production and Ellenburger saltwater disposal (i.e., Denton, Wise, Jack, Parker, Tarrant, Johnson, and Hood Counties) and extends westward across the Bend Arch to capture variability in flow properties throughout the region. Other study area boundaries are the Muenster and Red River Arches to the northeast and north, the Ouachita Thrust-and-Fold Belt to the east, and the Llano Uplift to the south (Figure 4).

Stratigraphic correlations

Within the study area, digital and raster logs were sourced from the Railroad Commission of Texas (2016) and IHS LogNet with a focus on (1) core production and disposal areas within the FWB, (2) well depth

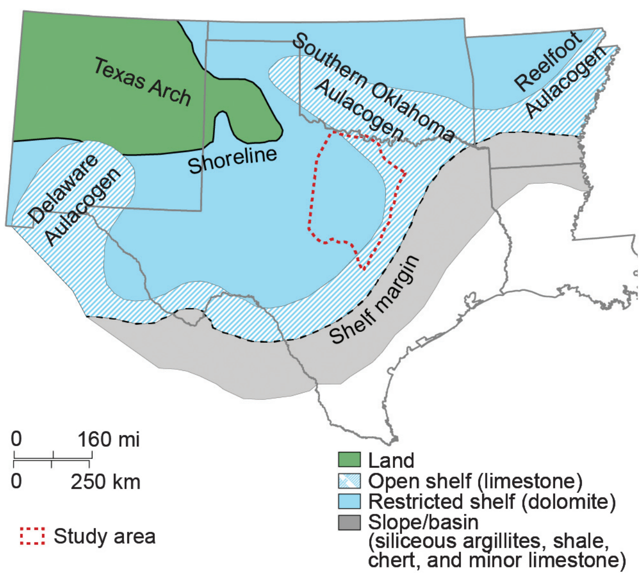

Figure 2. Lower Ordovician paleogeography, paleogeographic lithofacies (Ross, 1976), and interpreted regional depositional setting (Kerans, 1990); the study area is outlined in the dashed red line.

and intervals logged, and (3) log curve availability and quality. Wells penetrating basement were identified, and logs were sourced to provide structural control of the basement top surface and to characterize basement lithology.

Formation tops were correlated for 1286 wells (Figure 3) with digital logs across the FWB in IHS Petra v3.8.9. The Barnett Shale (including the Forestburg Limestone that separates the Upper and Lower Barnett), Viola-Simpson (undifferentiated), Ellenburger, and basement were correlated across the basin. All 1286 wells log the Barnett interval, 1023 wells penetrate Ordovician units (Viola-Simpson and/or Ellenburger), and 100 wells penetrate or nearly penetrate crystalline basement. The Ellenburger was subdivided into distinct lithostratigraphic units — primarily reflecting proportions of limestone and dolomite — and correlated across 40 wells with adequate depth and robust digital log suites.

Stratigraphic analyses were based on gamma ray (GR), resistivity (RES), bulk density (RHOB), neutron porosity (NPHI), and photoelectric factor (PEF) logs (Figure 3). Formation tops for the Ellenburger subunits and basement were adjusted based on the results of the petrophysical interpretation.

Identification of the Ellenburger subunits using raw logs is challenging, particularly when a PEF curve is not available. A new log N was computed to aid in identifying lithology and correlating subunits within the Ellenburger. Based on the density-neutron crossplots commonly used in carbonate systems, Burke et al. (1969) first propose the "lithoporosity" crossplot deriving porosity-independent N from the slope of the line from the matrix point (0% porosity) to the fluid point (100% porosity) for a given mineral (equation 1):

$$N = \frac{(\phi N)_f - \phi N}{\rho_b - \rho_f} \tag{1}$$

where ρ_b is the bulk density log, ϕN is the neutron poros log, and ϕN_f and ρ_f are the nominal neutron and density fluid responses (here, 1.0 decimal units and 1.0 g/cm^3,

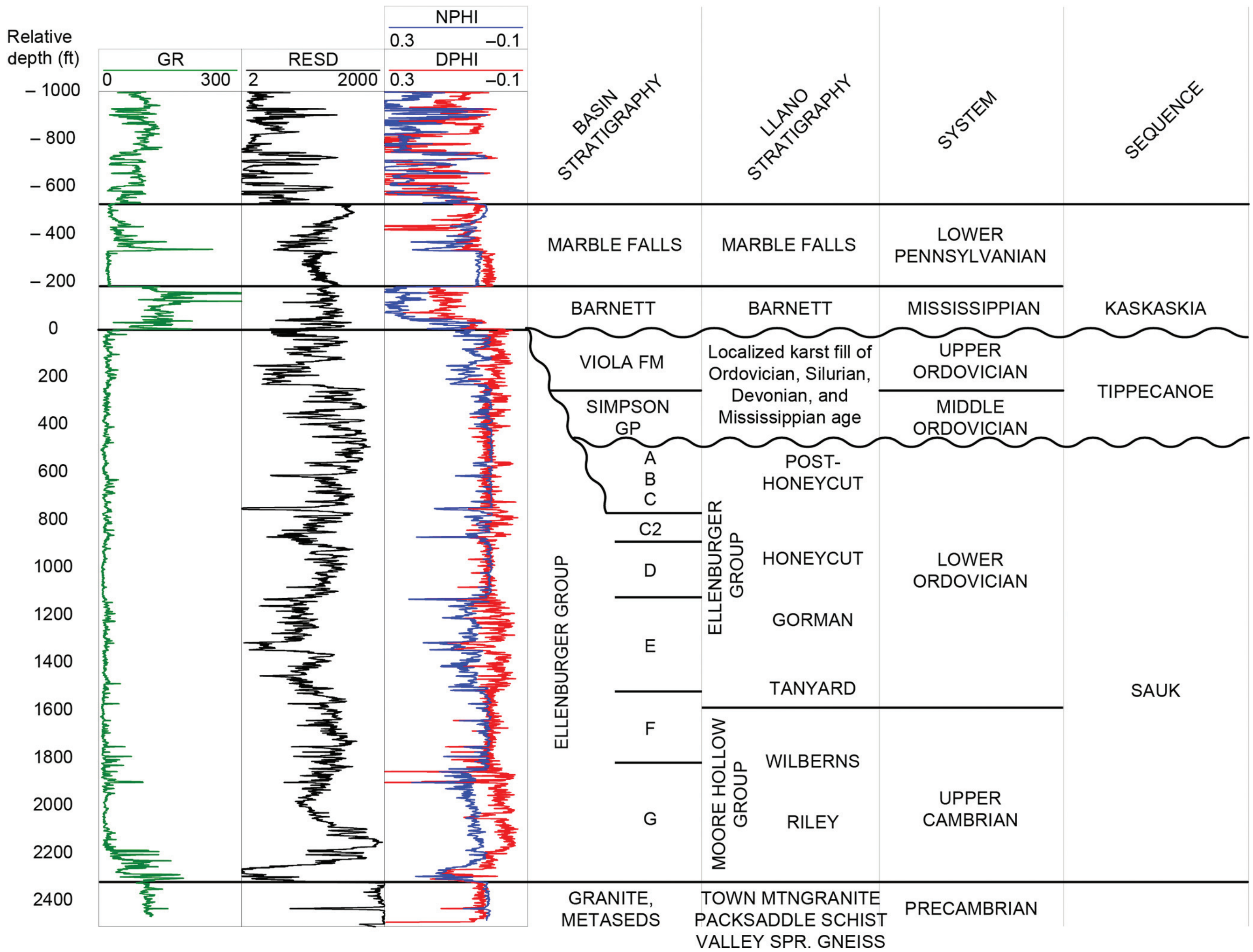

Figure 3. Type logs and general stratigraphic relationships within the basin (this study) compared to previous work on the Llano region (e.g., Barnes et al., 1959), and depositional sequence boundaries (Sloss, 1976). GR is gamma ray, RESD is deep resistivity, NPHI is neutron porosity, and DPHI is density porosity.

respectively). The resulting N log is used to check the calibration of porosity curves and to assess lithology, allowing for differentiation of limestone and dolomite for wells without PEF curves. Higher values of N (e.g., 0.60) reflect lithology that is dominantly limestone, whereas lower values of N (e.g., 0.52) correspond to dolomite.

Petrophysical interpretation

A subset (46) of the correlated wells (red dots in Figure 4) was selected for petrophysical interpretation of the organic-rich Barnett and Ellenburger Group carbonate intervals, based on depth and log curve availability. Of the wells studied, 20 contained GR, NPHI, RHOB, and PEF curves, whereas 20 lacked PEF curves and 6 contained only GR and RHOB curves. The resistivity log curve availability was variable.

Petrophysical interpretation was carried out in Interactive Petrophysics. A deterministic triple combo interpretation was used for the organic-rich Barnett interval. The clay volume V_{Clay} was interpreted using the neutron-density crossplot technique, and the remaining lithologic composition was interpreted using a matrix density-photoelectric absorption cross section (UMA-RHOMA) methodology assuming a constant kerogen density of $1.6\ \mathrm{g/cm^3}$. The total porosity was calculated using a density porosity equation with variable grain density.

For carbonate lithologies below the Barnett (Viola-Simpson and Ellenburger), a deterministic triple combo interpretation was also used. The V_{Clay} value was interpreted using single clay indicators GR, NPHI, and NPHI-DPHI, when suitable. The remaining lithologic composition was interpreted using UMA-RHOMA and NPHI-DPHI crossplot techniques. The total porosity in these low-porosity units was evaluated using an NPHI-DPHI porosity interpretation or a density porosity equation with variable grain density, inferred from categorization as limestone or dolomite from PEF logs or computed N log.

The deterministic approach for petrophysical interpretation of carbonate intervals described above was adequate to characterize the bulk of the sub-Barnett Paleozoic units; however, high residual errors were observed in wells that penetrate the base of the Ellenburger, Cambrian siliciclastics, and Precambrian basement. Furthermore, the available mudlogs and outcrop studies highlight the necessity of a detailed model that allows for testing of varying mineralogy and incorporates components characteristic of siliciclastic lithologies. A subset of wells (16) was selected for further study of the lithologic character of these units (the yellow diamonds in Figure 3); wells were selected based on depth of penetration, log suite availability and quality, and geographic location.

The mineral solver in Interactive Petrophysics was used to determine the lithologic character. Multiple logs were input to the solver, which determines a solution by minimizing an objective function. Two solver models were used: a general Ellenburger model containing calcite, dolomite, quartz, clay, and porosity, with feldspar added for some wells, and an arkose model containing quartz, feldspar, clay, hematite, and porosity (Table 1). This mineral assemblage is similar to granite, so differentiating granitic and arkosic rocks is dependent on the evidence of layering or elevated porosity. Additional minerals (e.g., ankerite and chlorite) were tested locally when input logs could not be reconstructed given the existing model mineral assemblage.

Mapping

Using a high-resolution digital elevation model (USGS, 2017), ground elevation values were sampled to points along Ellenburger outcrop in the Llano Uplift region and merged with the Barnett and Ellenburger depths for interpolation. Surface layers were interpolated using a natural neighbor (NN) algorithm in

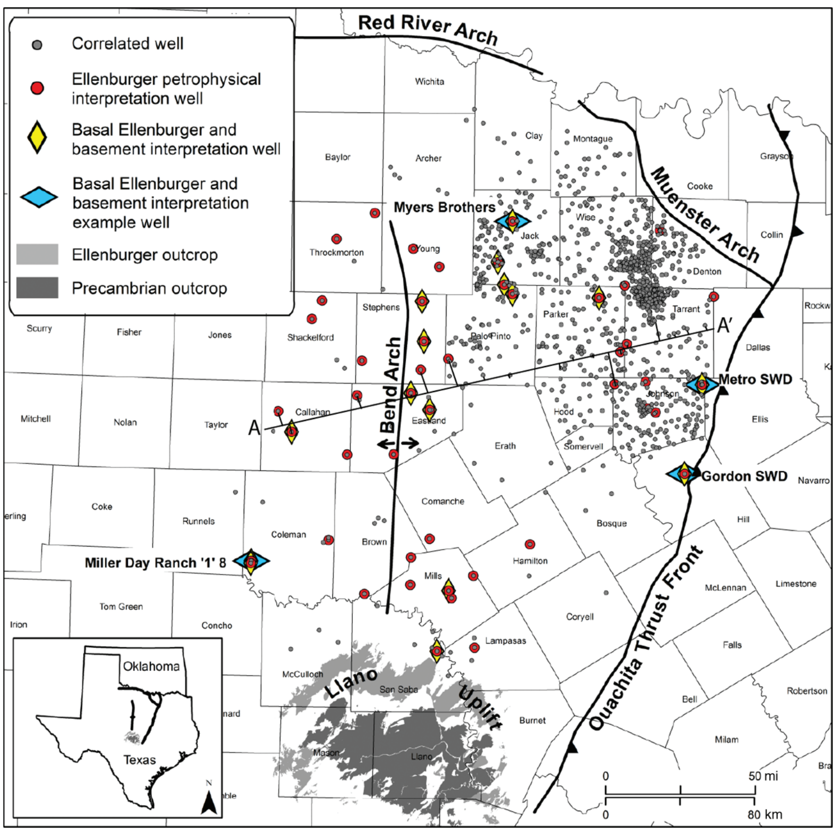

Figure 4. Study area with the major structural features and distribution of data including correlated wells (gray), wells used in petrophysical analysis of the Ellenburger (red), basal Ellenburger/basement interpretation wells (yellow), and location of example wells (blue) from Figure 6. Cross section A-A’ in Figure 8.

ArcMap v10.3. The NN algorithm only interpolates surfaces to the spatial extent of the data; to extrapolate to the full extent of the study area, a grid of points was created by sampling the NN raster values every 2000 ft (610 m). The grid values were then extrapolated to the extent of the study area boundary using an inverse distance weighted algorithm.

Because few wells log the entirety of the Ellenburger, additional indicators of lithology in the uppermost Ellenburger were mapped to assist in determining the Ellenburger stratigraphic architecture. The average GR for the top 20 ft (6 m) and the average N for the top 100 ft (30 m) of the Ellenburger were calculated and mapped. The disposal zone pore volume was computed in billion barrels on a square-mile block basis by extracting the average thickness and porosity for each block.

Results

Petrophysics

Of the 100 wells identified that penetrate or nearly penetrate basement, only half had adequate log suites for petrophysical analysis and correlation of the Ellenburger subunits. Ellenburger lithology, interpreted from a model containing calcite, dolomite, quartz, clay, and porosity, shows variable mineral composition alternating between calcite and dolomite as the main minerals, with a less frequent siliciclastic (quartz + clay) facies. The carbonate intervals are generally clean, with clay content less than 10 vol%. However, increased clay volume (up to 40 vol%) is observed at the top of the Ordovician. Porosity in the carbonate intervals is typically less than 5 p.u. with higher porosity in dolomite than in calcite. Porosity is highest where siliciclastic material is dominant (Figure 5), and porosity of up to 20 p.u. is observed in clean sandstone.

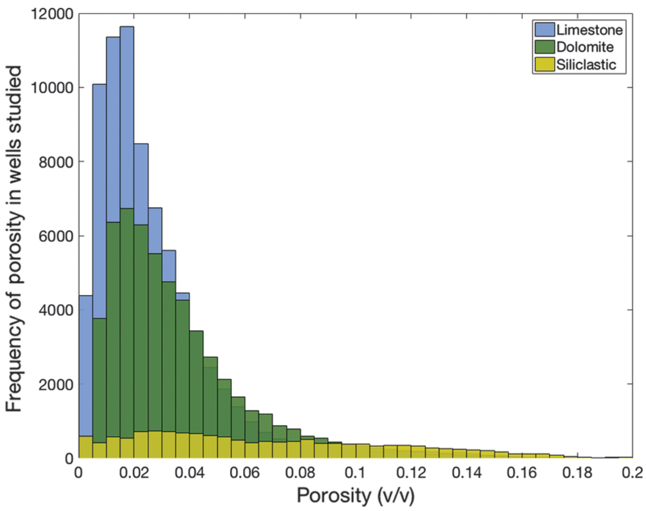

Figure 5. Distribution of porosity within the Ellenburger and Cambrian grouped by facies, showing higher porosities in siliciclastic facies relative to carbonates.

Basal Ellenburger, Cambrian, and basement lithologies vary when interpreted using combined carbonate and siliciclastic models, and no assemblage of minerals is sufficient to accurately characterize these units in all wells. Crystalline basement is identified by lithology and, importantly, very low porosity, verging on 0 p.u. (Figure 6a and 6b). In general, an increase in porosity is observed as the basement contact is reached (Figure 6b and 6c). Evidence of layering in the basal Ellenburger and Cambrian is also observed for some wells (Figure 6b). Where the model predicts granitic compositions coincident with appreciable porosity, the lithology is interpreted as a granite wash (Figure 6c). Hematite is frequently present in the interpretation of granite wash and crystalline basement and ranges from 5 vol% to 10 vol% locally, decreasing downward from the previously exposed top of basement (Figure 6a).

Four representative wells highlight the variable lithologic character across the basin. Gordon SWD 1 (Figure 6a) is located in Hill Co. in the southeast part of the study area along the Ouachita Thrust Front. Initial results with an Ellenburger model showed substantial input log reconstruction error below the top of basement; reconstruction error was minimized with inclusion of feldspar and hematite instead of calcite and dolomite. Basement lithology was identified as dominantly granitic, with muscovite probably making up the “clay” component. Elevated U (PEF) in the uppermost basement suggests the presence of an Fe-bearing mineral; 7 vol% hematite accounts for this response. Quartz sand is identified directly above basement, but the lithology is dominantly dolomite with small amounts of limestone and sandstone. This well shows

Table 1. Nominal petrophysical properties of minerals included in the Ellenburger and basement interpretation.

	Quartz	Calcite	Dolomite	Pyrite	Clay	Kerogen	PHIT	Feldspar	Biotite	Hematite	Ankerite
DPHI	0.035	0	−0.08187	−1.3392	−0.05263	0.8538	1	0.1111	−0.1460	−0.5725	−0.1889
NPHI	−0.035	0	0.035	−0.02	0.35	0.7068	1	−0.03	0.2	0.075	0.1
SPHI	0.03887	0	−0.03534	−0.07067	0.1943	0.8304	1	—	—	−0.03180	−0.00353
Vclay_GR	0	0	0	0	1	2	0	1	1	0	0
Vclay_ND	−0.1739	0	0.2903	3.2764	1	−0.3651	0	−0.3505	0.8592	1.6082	0.7175
U	4.5	15.5	9	80	8	0.22	0.22	7.2	20	110	22

no evidence of an arkose or sandy unit, or granite wash, overlying basement.

Of the wells studied to determine basement and basal Ellenburger lithologies, Metro SWD (Figure 6b) in northeast Johnson Co. shows the most complex lithology. A rare example of a basement penetration in the deepest part of the basin, it logs 4240 ft (1290 m) below the Barnett. With implementation of the Ellenburger mineral solver model, substantial error in reconstruction of input logs was observed for the basal 70 ft (21 m). An improved model required addition of a dense mineral with high-U (PEF) and low-GR response. Although hematite does not account for the log response, inclusion of ankerite — with properties of 3.0 g/cm^3 RHOB, NPHI of 0.1 and U of 18 — led to reduced error through 12,758 ft (3889 m) MD, just above basement. Below this, a 4–5 ft (1.2–1.4 m) thick sandstone is interpreted, which overlies another 4–5 ft (1.2–1.4 m) ankerite-rich interval. These layered lithologies are overlying basement rock that appears to be metamorphosed, containing quartz, feldspar, and chlorite. Biotite, calcite, and hematite were all tested as possible components in the model; clay was included but none was computed.

Initial analysis of Myers Brothers in central Jack Co. (Figure 6c) revealed high input log reconstruction error below 8415 ft (2565 m) MD when a carbonate model was used. Although inclusion of feldspar resulted in reduced errors, this arkose model did not satisfactorily describe the observed lithologies. The quartz- and feldspar-rich lithology penetrated at well total depth is likely sedimentary, as evidenced by the presence of porosity; the mineral constituents resemble granite so a granite wash is interpreted rather than crystalline basement rock.

Miller Day Ranch "1" 8 in the western part of the basin near the Llano Uplift (Figure 6d) does not penetrate the crystalline basement, but it does log most of the Ellenburger and Cambrian. The model applied included calcite, dolomite, quartz, feldspar, clay, and porosity. In contrast to other wells analyzed, which lack true porous sands, this well contains approximately 60 ft (18 m) of sandstone with 15 p.u. porosity. A nearby well, Miller Day Ranch "1" 9, is the only other well studied that also logs appreciable porous sands.

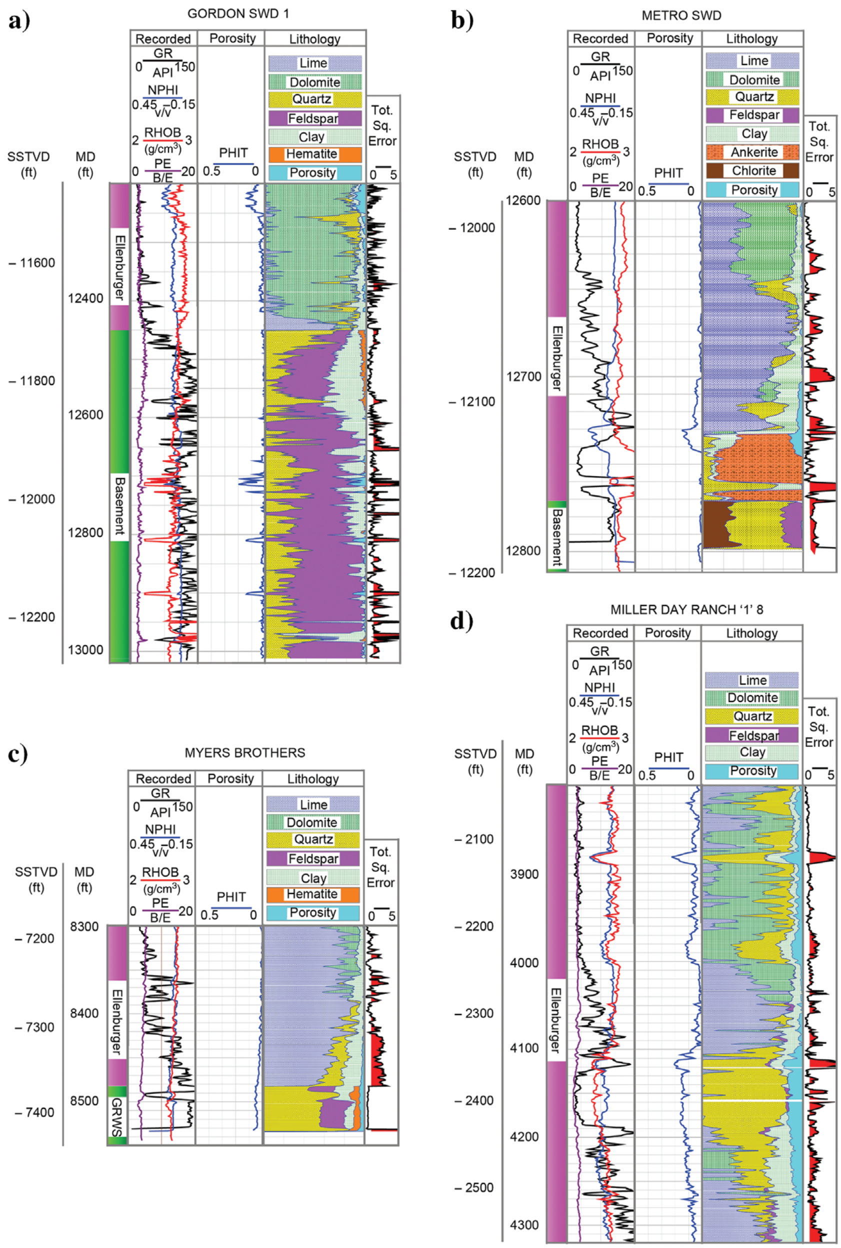

Figure 6. Petrophysical interpretation of Ellenburger, Cambrian, and basement lithology for (a) Gordon SWD 1, (b) Metro SWD, (c) Myers Brothers, and (d) Miller Day Ranch "1" 8. GR is gamma ray, NPHI is neutron porosity, RHOB is bulk density, PE is photoelectric curve, and PHIT is total porosity computed from the log model.

Stratigraphy, structure, and thickness mapping

Stratigraphy

The Barnett Shale is differentiated from the overlying Marble Falls Formation and underlying carbonates of the Viola, Simpson, and Ellenburger based on its high GR signature (up to approximately 250 American Petroleum Institute (API) units), originating primarily from uranium associated with total organic carbon, and its low bulk density (approximately 2.5 g/cm^3) due to the presence of low-density kerogen (commonly approximately 1.6 g/cm^3). A "gas effect" is observed in the response of the neutron and density log curves such that they approach one another and, in some instances, overlap (Fu et al., 2015).

The Viola and Simpson are identified beneath the sub-Barnett unconformity in the northeast part of the basin. In general, the Viola presents as a massive, clean, tight limestone with low GR, high resistivity, and low neutron and density porosity. The Simpson, with its more abundant shale content, has a higher GR response than the Viola. For the purposes of this study, the Viola and Simpson were correlated and mapped together.

Because many of the logged wells in the FWB core producing area were drilled as vertical pilot holes for producing Barnett wells, they often only penetrate the formation directly underlying the Barnett. Fewer than 100 Ellenburger penetrations are identified in which the Viola-Simpson is present, but additional data, including mud logs, are incorporated for added structural control. Throughout most of the basin, where the Viola and Simpson are absent, the Ellenburger is easily differentiated from the overlying Barnett based on its low GR (<50API), high bulk density (approximately 2.75 g/cm^3), and low neutron porosity (<0.10 v/v). The top of the basement was identified where the petrophysical interpretation indicated the presence of crystalline rock, and by its high GR, high resistivity, and very low porosity. An overlying granite wash, not present everywhere, was noted but not mapped.

The Ellenburger was divided into lithostratigraphic subunits based on the interpreted lithology and properties influencing fluid flow such as porosity. Eight distinct units were identified (Figure 7). In general, the alternating limestones and dolomites are correlative across much of the basin. Although facies vary laterally, the properties of each unit can be generalized. The basal unit, Ellenburger G, shows the most variation in lithology. It includes siliciclastic material that is likely Cambrian in age toward the west and southwest parts of the basin. The siliciclastic facies is the most porous and permeable of the disposal stratigraphy, and it grades laterally into carbonate — dominantly dolomitic — lithologies toward the north and east. The porosity of this unit averages 5.4 p.u. Near the Llano Uplift, local subsurface log correlation of the Cambrian siliciclastic units is possible, as is tying the units to formations within the Moore Hollow Group, but the lateral facies variation and lack of deep well penetrations mean that only the carbonate section can be correlated throughout the entire basin.

Ellenburger F is a laterally continuous limestone with porosity averaging 3.0 p.u. Ellenburger E is a dolomite to mixed dolomitic limestone, with the dolomite volume making up 0.49 v/v on average. Ellenburger D, which is only present locally, is a tight limestone (1.5 p.u. porosity, 0.118 v/v dolomite), and it is evidence of lateral facies changes. Ellenburger C2 is dolomitic, and it is only present east of the Bend Arch, along with the overlying Ellenburger C. Elsewhere, these units have been eroded. Ellenburger C is mostly limestone, with a dolomitic marker at the top. It has porosity of 1.6 p.u. and dolomite volume fraction of 0.26 v/v. Ellenburger B is a limestone with 1.1 p.u. porosity and 0.185 v/v dolomite. Ellenburger A is a mixed dolomite-limestone, with 1.8 p.u. porosity on average, and a dolomite volume fraction of 0.511 v/v. Ellenburger A and B are only present in the eastern part of the basin, and the complete section of Ellenburger A is only observed where the Viola and Simpson are present.

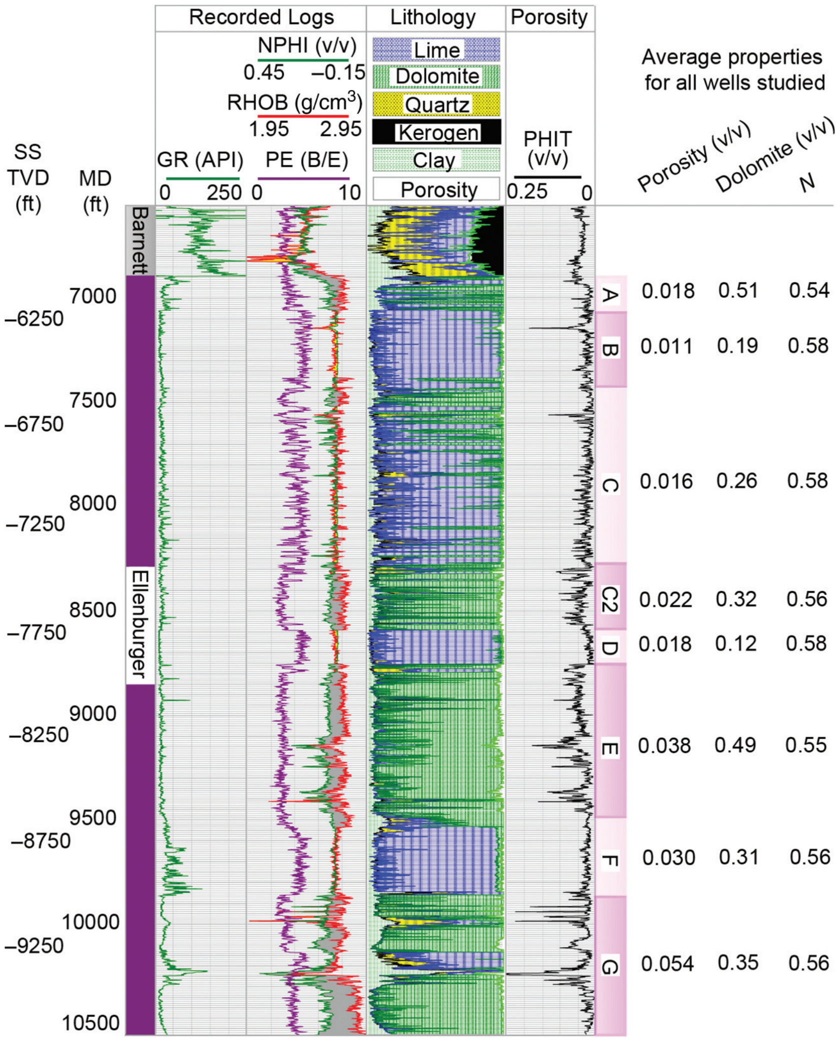

Figure 7. Ellenburger type log showing interpreted lithology (limestone in blue and dolomite in green) and lithostratigraphic subunits A–G with average values for porosity, dolomite volume, and *N* (Burke et al., 1969).

Structure trends

The Barnett, Ellenburger, Viola-Simpson, and basement units are shallowest to the west and southwest (over the Bend Arch and near the Llano Uplift), and they deepen toward the east and northeast (near the Ouachita structural front and Muenster Arch) (Figure 8). The structure on the top of the Ordovician (Figure 9a) is the base of the Barnett, and it is equivalent to the top of the Ellenburger throughout most of the basin and Viola or Simpson where present in the deepest parts of the basin along the Muenster Arch. The top of the Ordovician represents the top of the disposal stratigraphy. The contours reflect major structural features, including the Bend and Lampasas Arches and the Mineral Wells fault system. The elevation of the top of the Ordovician ranges from outcrop at the Llano Uplift to −7800 ft (−2377 m) subsea along the Tarrant-Dallas county line.

The basement surface (Figure 9b) was mapped based on 56 wells that penetrate the crystalline basement, and the elevation ranges from outcrop at the Llano Uplift to −12,200 ft (−3719 m) in northeast Johnson Co. Although lacking well control in the deepest parts of the basin, the basement surface deepens further toward the Ouachita structural front (Figure 8).

Thickness and porosity trends

The thickness of the Barnett Shale is approximately 50 ft (15 m) across much of the basin, thickening toward the Muenster Arch to >1000 ft (305 m). The intervening Forestburg Limestone, dividing the Barnett into Upper and Lower Units, centers on Wise County and reaches approximately 300 ft (91 m) in thickness. The Viola and Simpson Formations underlying the Barnett were mapped together. They reach a total thickness of more than 750 ft (229 m) along the Muenster Arch and pinch out along a line trending roughly northwest–southeast through Wise, Tarrant, and Johnson Counties. The combined Ellenburger and Cambrian thickness (Figure 10a) increases from <1500 ft (457 m) west of the Bend Arch to >4000 ft (1219 m) along the Muenster Arch and Ouachita Thrust Front, and it represents the injection envelope for disposal wells in the Ordovician and Cambrian. Pore volume (porosity × thickness) of the disposal interval (Figure 10b), while reflecting the thickness along the Muenster Arch, is primarily driven by high-porosity siliciclastic facies in the southwestern part of the study area.

Discussion

The Ordovician and Cambrian disposal intervals in the FWB overlie a basement that is laterally heterogeneous, consisting of metasedimentary, igneous, or metamorphosed igneous lithologies. Although sampling few wells, the interpreted basement lithology for wells in this study is dominantly granitic, consistent with previous studies on outcrop and in the subsurface that indicate that plutonic rocks and metamorphosed plutonic rocks make up the vast majority of the Texas Craton (e.g., Flawn, 1956).

The complexity of basement and overlying lithologies, combined with the lack of well penetrations, means that regional mapping of lithologic variation is not feasible on a basin-wide scale. One challenge of constraining lithology of the basement is the sensitivity of computed mineral volumes to log normalization. GR logs are normalized to clay volume computed from neutron density in the Barnett, with the effect of causing variation in the feldspar volume in basement. Relative calibration of neutron and density logs also poses a challenge; although computed N (Burke et al., 1969) may indicate a need for calibration, it also reflects

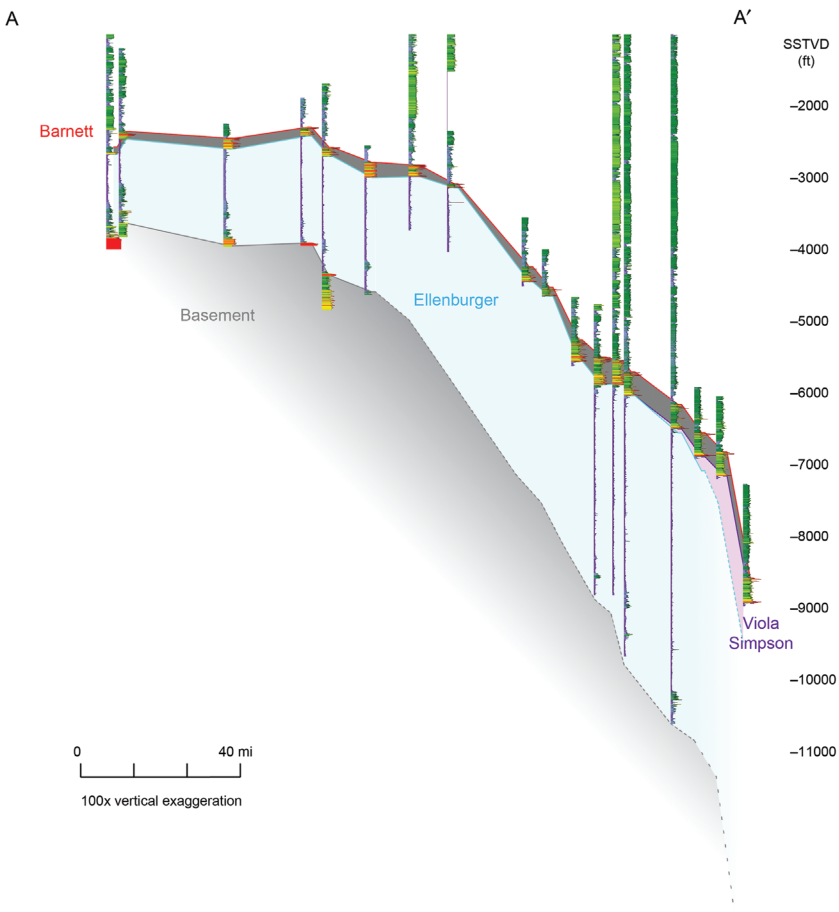

Figure 8. Structural cross section (west–southwest to east–northeast) showing the Barnett, Viola-Simpson, Ellenburger, and basement deepening, and thickening, toward the northeast. The gamma ray log is displayed, showing high (hot) values for the Barnett and crystalline basement. The section line shown in Figure 4.

variations in calcite and dolomite in the Ellenburger. Miscalibration of the density log results in variations in the hematite volume computed. Another challenge in determining the lithology of basement rocks — specifically in differentiating crystalline basement from arkosic sedimentary rocks — is that the petrophysical logs do not provide information about texture. When lithologies are similar (i.e., for granite and granite wash), the interpretation depends on evidence of layering or the presence of porosity to determine the rock type. Granite wash overlying crystalline basement is not a universal finding across the basin, but it is observed in isolated wells. Its distribution and thickness cannot be mapped or predicted, and it may reflect local paleotopography and proximity to nearby buried granite hills (Barnes et al., 1959).

Basal sands of the Cambrian are usually arkosic, containing some feldspar, and we identify them as a siliciclastic facies that is a lateral variation of what is dominantly carbonate toward the east (Figure 11a)

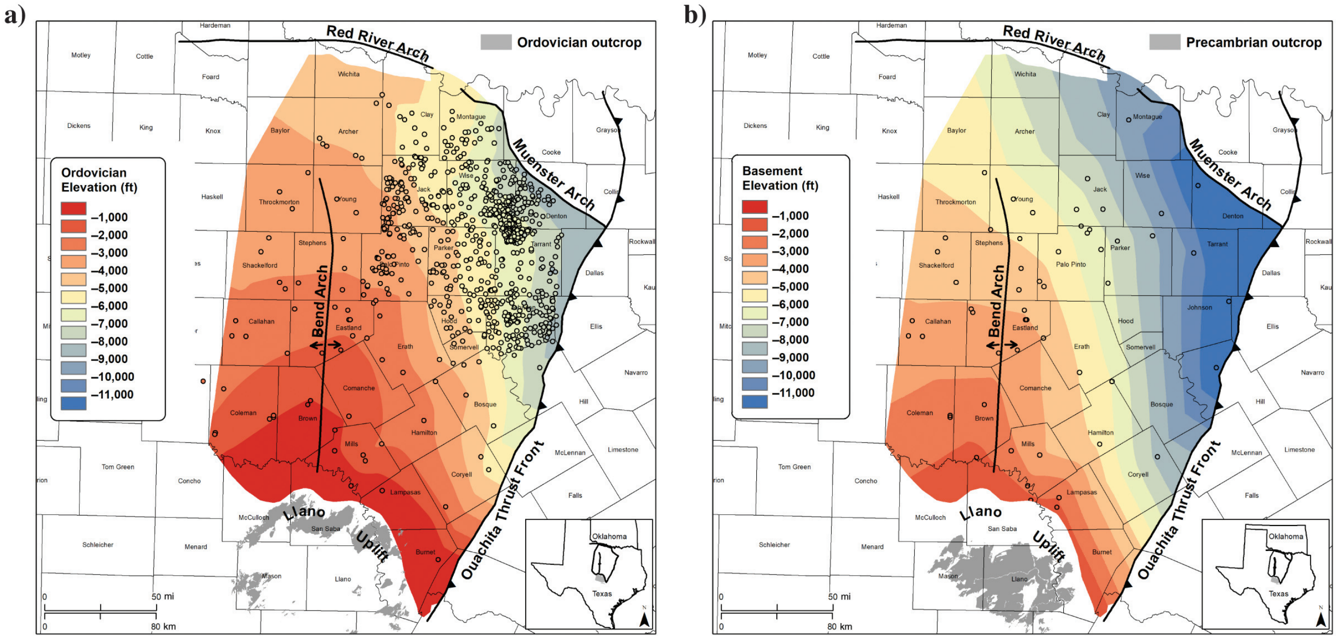

Figure 9. Elevation (ft subsea) of top of (a) Ordovician and (b) basement, constrained by 1023 and 56 wells, respectively.

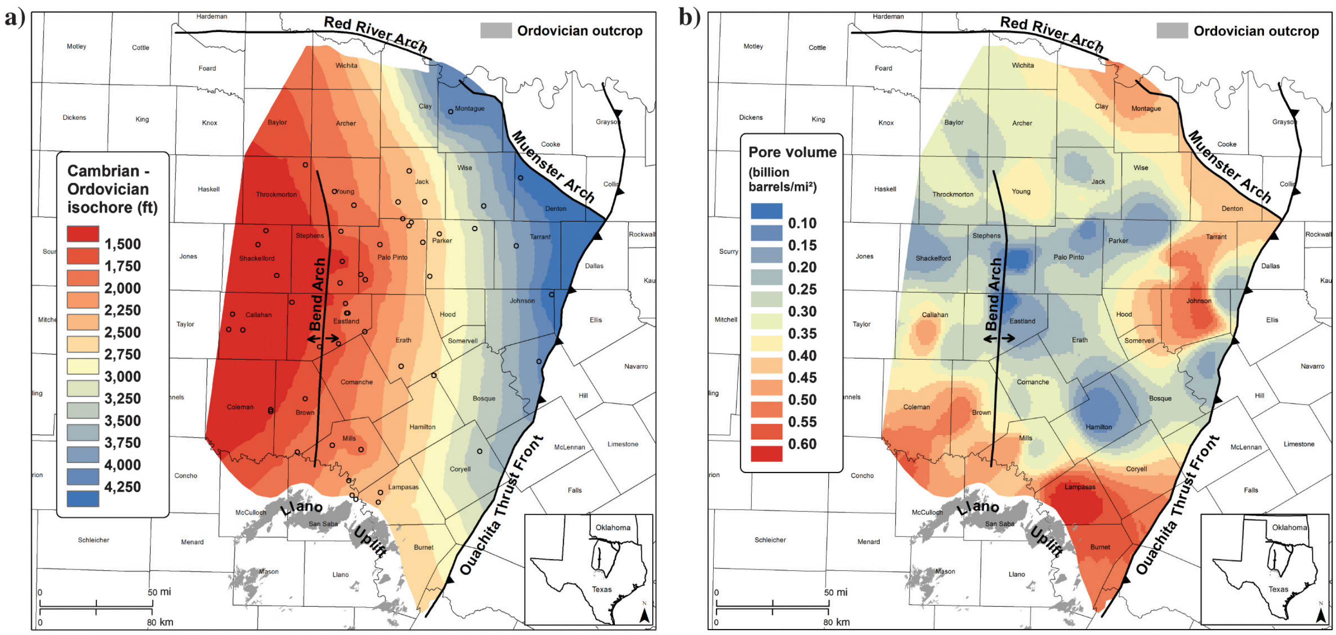

Figure 10. (a) Total thickness of the combined Ordovician and Cambrian units (from the crystalline basement to the Barnett Shale, including the Viola-Simpson, Ellenburger, and Cambrian siliciclastics) and (b) total pore volume (porosity × thickness) of the Ordovician and Cambrian disposal interval.

The siliciclastic facies is often approximately 80 ft (24 m) thick in sampled wells. This lithology (containing quartz, feldspar, and clay) is consistent with previous work on the Hickory (the basal member of the Riley Formation), which is dominantly quartz with feldspar only locally important at the base, probably due to proximity to granite (Barnes and Bell, 1977), and which contains minor amounts of siltstone and shale (Pettigrew, 1991). The Riley Formation has been hypothesized to either lap out against basement rocks approximately 100 mi (160 km) northeast of the Llano uplift (e.g., Barnes et al., 1959) or to extend northeastward into the basin (e.g., Bradfield, 1964). We only observe this facies approximately 100 mi (160 km) north of Llano; the extent to the northeast is poorly constrained due to well control, but the basal siliciclastic facies laps out southeast of Hill Co. and is not observed in the deeper parts of the basin.

The distribution of siliciclastics within the disposal stratigraphy exerts control on the disposal interval pore volume, which is greatest to the west and southwest where siliciclastic facies make up a greater portion of the disposal stratigraphy. The region of high pore volume is also where near-basement Hickory sandstone saltwater disposal occurs. Based on the map of structure on the top of the basement, the vertical distance from the bottom of the disposal interval to the basement ranges from 0 to 3182 ft (0–970 m) with a mean of 636 ft (194 m) throughout the study area, but where siliciclastic facies are present many injection wells are within approximately 50 ft (15 m) of the mapped basement surface.

The siliciclastic facies above the basement is distinct from the porous sands infrequently encountered in the wells studied; only in the Miller Day Ranch area is this lithology observed, and these wells are the furthest west in the study area. In each well, two sandstone beds are separated by approximately 100 ft (30 m) of carbonate, and they also overlie a carbonate layer, in contrast to the basal siliciclastic facies that overlies basement. These sands are not likely to be equivalent to the Hickory, but rather are stratigraphically higher, and they are lateral facies variations within a layer that gives way to carbonate toward the east. Cornish (1975) suggests that sandstones northwest of Llano are lateral facies variations of members overlying the Hickory. The position of the Cambrian shoreline supports this interpretation because the Cambrian siliciclastics have been shown to be almost entirely sourced from the granite-rhyolite province and transported by paleorivers draining the Texas Arch (Alsalem et al., 2017).

Carbonates of the Ellenburger are continuous compared to siliciclastics (Figure 11b) and therefore can be correlated on a basin-wide scale, although lateral facies changes and local erosion pose challenges. Deposition of the carbonates occurred on a laterally extensive carbonate platform along the edge of Laurentia. In contrast to the almost entirely dolomitized Ellenburger of the Permian Basin region, limestone is abundant in the FWB, where alternating limestone and dolomite facies are observed. There is no evidence of increasing limestone volume fraction indicative of the outer rim of more open-shelf deposits toward the east as proposed in paleofacies (Ross, 1976) and inferred depositional environments (Kerans, 1990) for the Permian Basin region.

In the Permian Basin, several stages of dolomitization and multiple episodes of karsting have been identified, including a several-million-year hiatus and exposure of the Ellenburger Group at the end of the Early Ordovician (Kerans, 1988, 1989; Lucia, 1995; Loucks, 1999). This unconformity corresponds to the boundary between the Sauk (Cambrian and Early Ordovician Ellenburger) and Tippecanoe (Middle

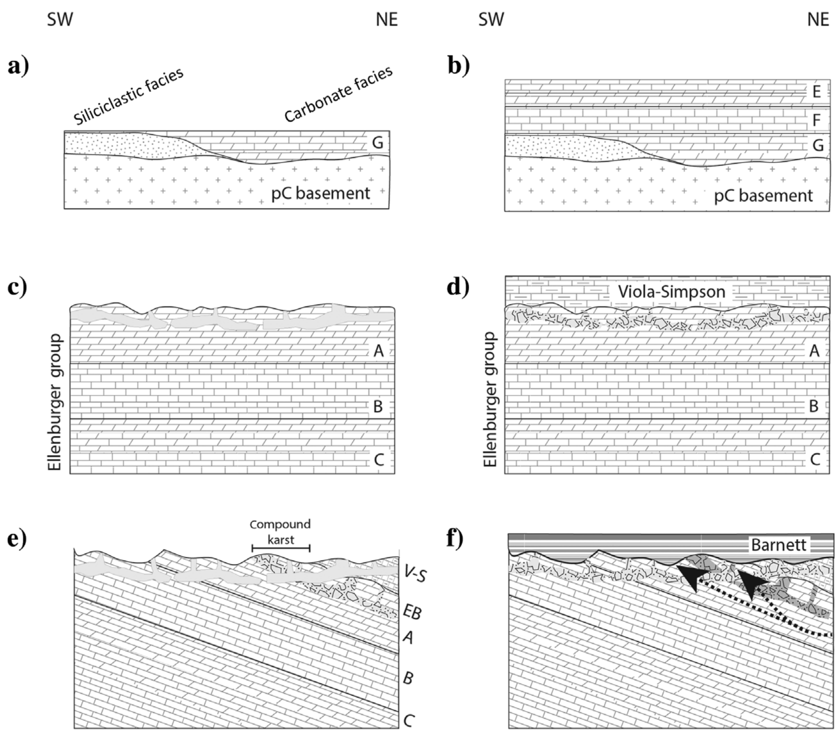

Figure 11. Depositional history of the FWB disposal stratigraphy. (a) Cambrian siliciclastic facies toward the west and southwest give way to carbonate toward the east, (b) laterally extensive Ellenburger carbonates are deposited, (c) at the Sauk-Tippecanoe unconformity (end of the early Ordovician), exposure of the Ellenburger A and extensive karsting, (d) the Simpson Group and Viola Formation are deposited upon the karsted Ellenburger A surface, (e) Uplift and erosion of Ordovician (and any younger) rocks, and extensive karsting at the Tippecanoe-Kaskaskia sequence boundary, and (f) deposition of the Mississippian Barnett Shale, along with expulsion of fluids associated with Ouachita thrusting.

Ordovician Simpson and Viola) sequences of Sloss (1976). The shelf deposits (e.g., Ellenburger) in the Permian Basin region were exposed, whereas the slope deposits (e.g., of the Marathon Basin and Southern Oklahoma Aulacogen) remained submerged (Kerans, 1990). The presence of karsting in the Ellenburger Group in the FWB suggests that this area was also exposed. The youngest Ellenburger subunit (A) would have been extensively karsted at the Sauk-Tippecanoe unconformity (Figure 11c). In the Permian region karst affected strata at least 300–1000 ft (91–305 m) beneath the unconformity (Kerans, 1988, 1989; Lucia, 1995; Loucks, 1999).

Middle Ordovician Simpson equivalent and Viola Limestone were deposited atop this karsted Ellenburger A surface (Figure 11d). Uplift and erosion removed any Silurian and Devonian, much of the Viola and Simpson, and the upper part of the Ellenburger (A and B)

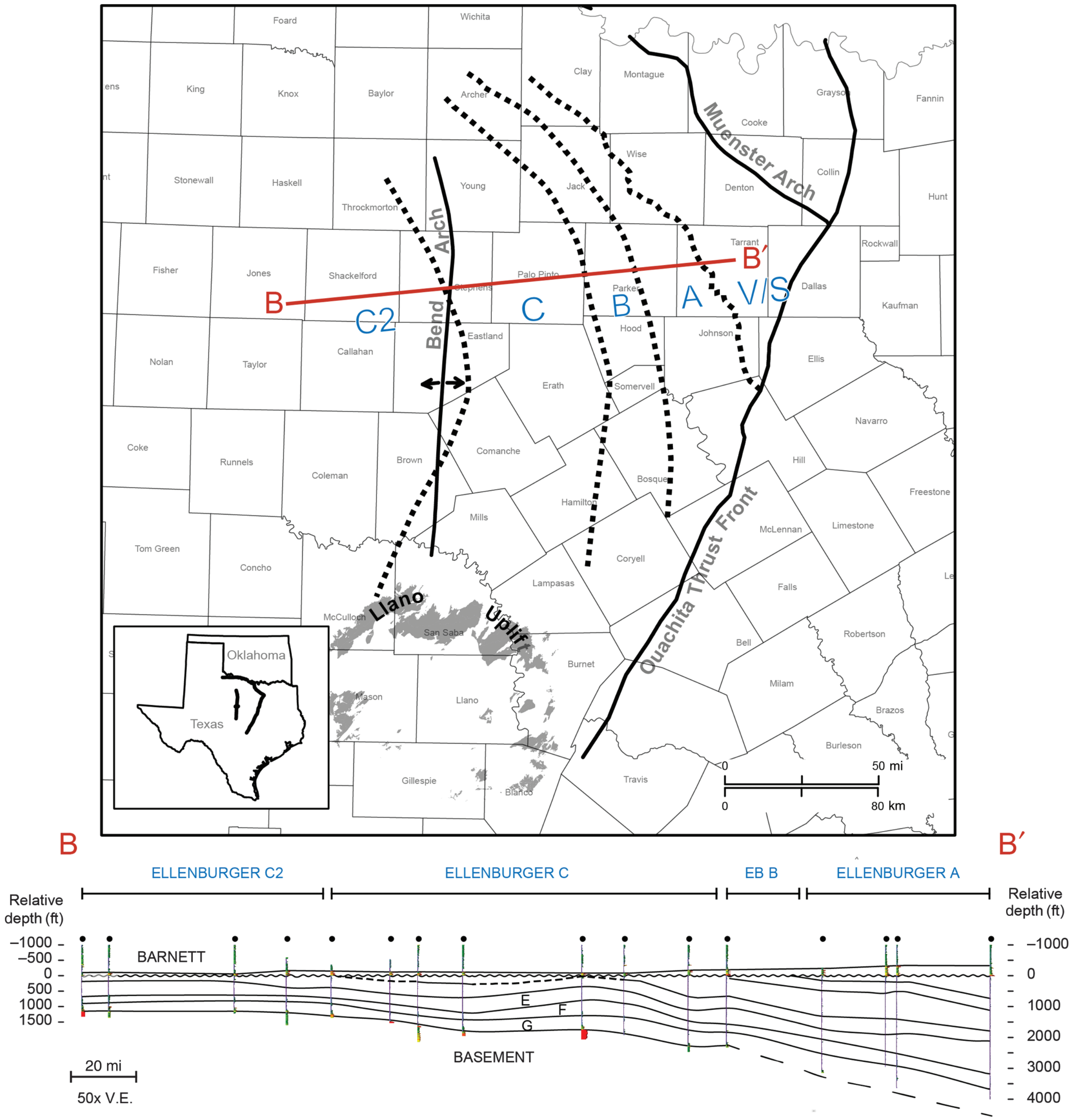

Figure 12. Pre-Barnett subcrop unit patterns showing the presence of the Viola-Simpson and Ellenburger A–C2 underlying the Barnett. Cross section shows the gentle angular unconformity between the Ordovician units and the overlying Barnett Shale.

throughout most of the FWB region (Figures 11e and 12); most erosion took place toward the west and southwest. This Ordovician-Mississippian unconformity marks the boundary between the Tippecanoe and Kaskaskia sequences (Sloss, 1976).

Although other periods of exposure and karsting likely took place throughout Ellenburger deposition, the most extensive karsting is expected where the Ellenburger A is present beneath the Barnett due to multiple episodes of exposure. The unconformity between the Ordovician and Mississippian is gently angular in the FWB, with a dip difference between the Ellenburger/Viola/Simpson and Barnett of 0.5°–1°. Assuming that up to 1000 ft (305 m) of the top of the Ellenburger A was affected by karsting at the earlier Sauk-Tippecanoe unconformity, and with a present differential dip of 0.5°–1°, a band of reexposed Ellenburger 10–20 mi (16–32 km) wide would be expected adjacent to the Viola-Simpson subcrop line. This dolomitized porous zone would have served as a preferential pathway for migration of hydrothermal fluids expelled from basinal shales during Ouachita thrusting (Kupecz and Land, 1991) (Figure 11f).

The Ellenburger strata underlying the Barnett are progressively older toward the west (Figure 12), reflecting the shallow angular unconformity between the Barnett and Ordovician Formations as the younger units were progressively eroded toward the west. The uppermost Ellenburger layers — A and B, together more than 1000 ft (305 m) thick in the deepest part of the basin — are only observed in the subsurface, and their subcrop patterns roughly correspond to those of the post-Honeycut beds predicted by Hendricks (1964) to exist in the subsurface of the FWB.

The high dolomite volume fraction within the Ellenburger is indicated by low values of N (approximately 0.52 for dolomite and 0.60 for limestone). The Ellenburger directly underlying the Barnett is increasingly dolomitized toward the east where the youngest Ellenburger beds are present (Figure 13a). The mapped GR in the top 20 ft (6 m) of the Ellenburger reveals a band of increased GR in which the Ellenburger A is present (Figure 13b). The high GR in the uppermost Ellenburger has been attributed by previous authors to invasion of dissolved uranium salts sourced from the Barnett into porous dolomite beds (Henry, 1982), although cave fill of shalier Simpson lithologies could also cause this log response. In the Ellenburger of the Permian Basin, comparison of log responses and core descriptions of karsted Ellenburger reveals a higher GR zone of cave-sediment fill in the upper Ellenburger above a layer of chaotic breccia (Kerans, 1989). Intense dissolution can result in the formation of cave fill breccias with higher porosity than the matrix, which can act as pathways for dolomitization (Kupecz and Land, 1991; Sullivan et al., 2006). In either case, the high-GR and low-N patterns reflect exposed and more intensely dolomitized layers. Sullivan et al. (2006) suggest that karst formation was most intense below the Mississippian (i.e., Tippecanoe-Kaskaskia) unconformity compared to the Middle Ordovician (Sauk-Tippecanoe) unconformity, and that in 3D seismic surveys in which the Upper Ordovician carbonates are present (i.e., where Viola-Simpson is beneath Barnett), Lower Ordovician Ellenburger carbonates have a lower density of sinkhole-like features. This work is consistent with that interpretation but furthermore suggests that a higher density of karst features is not expected

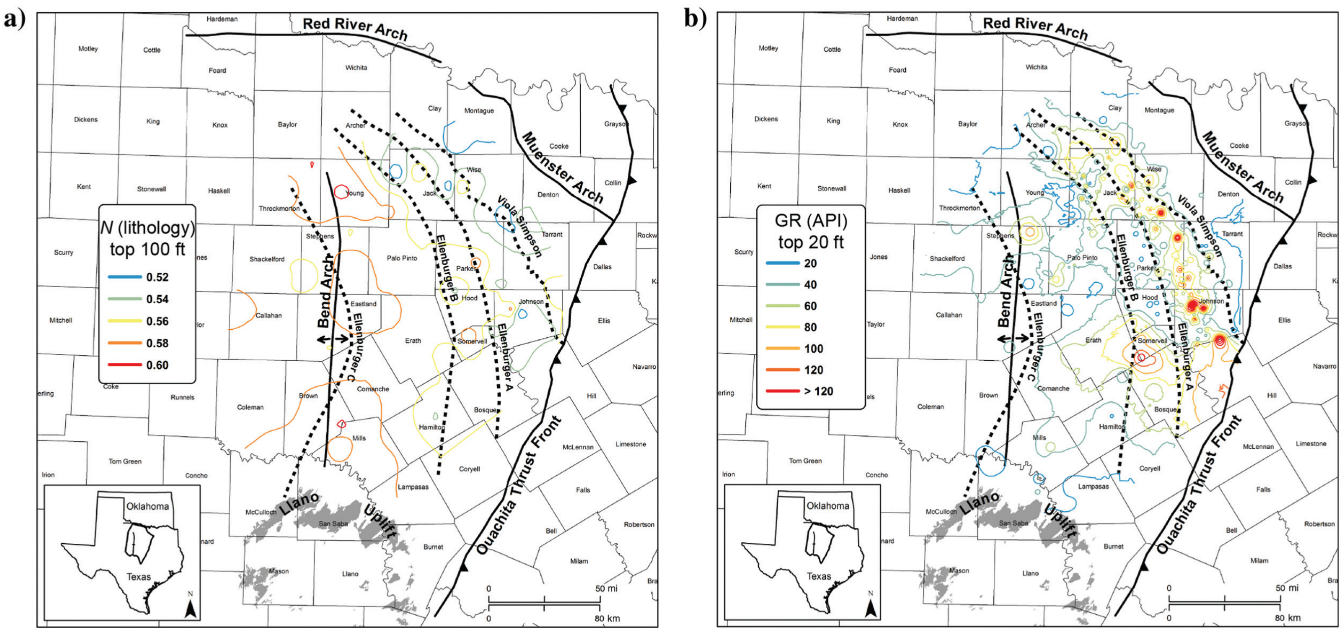

Figure 13. (a) Average N of the upper 100 ft of the Ellenburger showing the distribution of facies from limestone (high N) to dolomite (low N) from west to east and (b) average gamma ray of the top 20 ft of the Ellenburger showing a band of high-GR values in which the Ellenburger A is present beneath the Barnett.

everywhere the Lower Ordovician is present beneath the Barnett, but primarily where the previously exposed surfaces are composite.

Summary

This study presents the first basin-wide subsurface characterization of the deep disposal intervals of the FWB and their relation to basement. The stratigraphic architecture of Ordovician and Cambrian formations, and their facies and porosity distributions, may influence the flow of disposed fluid and potential pore pressure increases leading to induced seismicity. An understanding of the character of basement rocks and the basement-sediment interface is critical in determining the effect of disposal proximal to basement on basement-rooted faults. Key findings of this work that improve understanding of the disposal interval geology are summarized:

- Lithology of the crystalline basement of the FWB is varied and includes igneous, metamorphosed igneous, and metasedimentary rocks. The basement surface shows evidence of weathering with hematite (5–10 vol%) decreasing downward. Petrophysical analysis of basement penetrations requires an interpretive log model that allows for testing of varying mineralogy and incorporates components characteristic of siliciclastic lithologies.
- The character of the basement-sediment interface is equally complex. Rocks overlying basement can be granite wash, arkosic sedimentary rocks, porous quartz sands (western FWB), or carbonates (eastern FWB). The basement-sediment interface is frequently marked by increased porosity.
- Ellenburger lithology consists of dominantly calcitic or dolomitic intervals that are generally clean (clay <10 vol%) with low (<5 p.u.) porosity. In contrast to the Ellenburger of the Permian Basin, here the Ellenburger contains significant low-porosity tight limestone alternating with higher porosity dolomitized beds. Siliciclastics are more abundant in the western part of the basin, consistent with studies on the provenance of Cambrian sediments.
- Stratigraphic correlation of the laterally continuous dolomite and limestone beds reveals the internal architecture of the Ellenburger. A gentle angular unconformity between Ordovician Ellenburger, Viola, and Simpson, and the overlying Mississippian Barnett, with erosion greatest toward the west, means that the uppermost Ellenburger (A and B) is only observed in the subsurface of the FWB.
- Facies present at the top of the eroded Ellenburger are calcitic toward the west and dolomitic toward the east. A high GR signature at the top of the Ellenburger adjacent to the Viola-Simpson pinchout line is consistent with this Ellenburger layer having been exposed at least twice, with the most significant unconformities occurring between Early and Middle Ordovician (Sauk-Tippecanoe), and Middle Ordovician and Mississippian (Tippecanoe-Kaskaskia).

Acknowledgments

This work was funded by the State of Texas through the TexNet Earthquake Monitoring and Research Program. K. Smye is grateful to B. Berend and D. Loughry for helpful discussions. L. Sivila contributed to petrophysical analysis of carbonate intervals. Includes content supplied by IHS Global Inc. and copyright IHS Global Inc., 2018. All rights reserved. Please contact the corresponding author for access to GIS shapefiles from this study. The authors are grateful to the three reviewers whose feedback greatly improved the clarity of the manuscript.

Data and materials availability

Data associated with this research are available and can be obtained by contacting the corresponding author.

References

Adams, D. C., and G. R. Keller, 1996, Precambrian basement geology of the Permian basin region of West Texas and eastern New Mexico: A geophysical perspective: AAPG Bulletin, **80**, 410–431.

Alsalem, O. B., M. Fan, J. Zamora, J. X. Xie, and W. R. Griffin, 2017, Paleozoic sediment dispersal before and during the collision between Laurentia and Gondwana in the Fort Worth Basin, USA: Geosphere, **14**, 325–342, doi: 10.1130/GES01480.1.

Barnes, V. E., and W. C. Bell, 1977, The Moore Hollow Group of Central Texas: The University of Texas at Austin, Bureau of Economic Geology, Report of Investigations 88, 169.

Barnes, V. E., P. E. Cloud, L. P. Dixon, Jr., R. L. Folk, E. C. Jonas, A. R. Palmer, and E. J. Tynan, 1959, Stratigraphy of the pre-Simpson Paleozoic subsurface rocks of Texas and southeast New Mexico: University of Texas at Austin, Bureau of Economic Geology Publication 5924, 294.

Bradfield, H. H., 1964, The Ellenburger Group of North Central Texas: Tulsa Geological Society Digest, **32**, 112–118.

Burke, J. A., R. L. Campbell, Jr., and A. W. Schmidt, 1969, The litho-porosity cross plot — A method of determining rock characteristics for computation of log data: Illinois Basin Regional Meeting, SPE, doi: 10.2118/2771-MS.

Clabaugh, S. E., and R. V. McGehee, 1962, Geologic history of Central Texas: Precambrian rocks of Llano region, *in* E. H. Rainwater and R. P. Zingula, eds., Geology of the Gulf Coast and Central Texas, and guidebook of excursions: Houston Geological Society Publication, 62–78.

Cloud, P. E., and V. E. Barnes, 1948, The Ellenburger Group of Central Texas: University of Texas Publication 4621.

Cloud, P. E., and V. E. Barnes, 1957, Early Ordovician sea in Central Texas, *in* J. W. Hedgpeth, ed., Treatise on marine ecology and paleoecology. Part 2: Geological Society of America Memoir 67V2, 163–214.

Cloud, P. E., V. E. Barnes, and J. Bridge, 1945, Stratigraphy of the Ellenburger Group in Central Texas — A progress report: University of Texas, Bureau of Economic Geology Publication 4301, 133–161.

Collier, H., 1983, The Ellenburger of Central and West-Central Texas: A literature review, Exploration in a mature area: Abilene Geological Society, 190–207.

Combs, D. M., R. G. Loucks, and S. C. Ruppel, 2003, Lower Ordovician Ellenburger Group collapsed paleocave facies and associate pore network in the Barnhart field, Texas, *in* T. J. Hunt and P. H. Lufolm, eds., The Permian Basin: Back to basics: West Texas Geological Society Publication 03-112, 397–418.

Cooke, F. A., D. S. Albaugh, L. D. Brown, S. Kaufman, J. E. Oliver, and R. D. Hatcher Jr., 1979, Thin-skinned tectonics in the crystalline southern Appalachians; COCORP seismic-reflection profiling of the Blue Ridge and Piedmont: Geology, **7**, 563–567, doi: 10.1130/0091-7613(1979)7<563:TTITCS>2.0.CO;2.

Cornish, F. G., 1975, Tidally influenced deposits of the Hickory Sandstone, Cambrian, Central Texas: Master's thesis, The University of Texas at Austin.

Crowley, A. J., and L. Hendricks, 1945, Lower Ordovician and Upper Cambrian subsurface subdivisions in North Central Texas: AAPG Bulletin, **29**, 413–425.

Flawn, P. T., 1956, Basement rocks of Texas and southeast New Mexico: The University of Texas Bulletin 5605, 261.

Frohlich, C., 2012, Two-year survey comparing earthquake activity and injection-well locations in the Barnett Shale, Texas: Proceedings of the National Academy of Sciences, **109**, 13934–13938, doi: 10.1073/pnas.1207728109.

Frohlich, C., H. DeShon, B. W. Stump, C. Hayward, M. Hornbach, and J. I. Walter, 2016, A historical review of induced earthquakes in Texas: Seismological Research Letters, **87**, 1022–1038, doi: 10.1785/0220160016.

Frohlich, C., W. Ellsworth, W. A. Brown, M. Brunt, J. Luetgert, T. MacDonald, and S. Walter, 2014, The 17 May 2012 M4. 8 earthquake near Timpson, East Texas: An event possibly triggered by fluid injection: Journal of Geophysical Research: Solid Earth, **119**, 581–593.

Fu, Q., S. C. Horvath, E. C. Potter, F. Roberts, S. W. Tinker, S. Ikonnikova, W. L. Fisher, and J. Yan, 2015, Log-derived thickness and porosity of the Barnett Shale, Fort Worth Basin, Texas: Implications for assessment of gas shale reserves: AAPG Bulletin, **99**, 119–141, doi: 10.1306/07171413018.

Hendricks, L., 1952, Correlations between surface and subsurface sections of the Ellenburger Group of Texas: The University of Texas, Bureau of Economic Geology, Report of Investigations 11, 44.

Hendricks, L., 1964, Stratigraphic summary of the Ellenburger Group of North Texas: Tulsa Geological Society Digest, **32**, 119–125.

Henry, J. D., 1982, Stratigraphy of the Barnett Shale (Mississippian) and associated reefs in the northern Fort Worth Basin, *in* C. A. Martin, ed., Petroleum geology of the Fort Worth Basin and Bend arch area: Dallas Geological Society, 157–178.

Hincks, T., W. Aspinall, R. Cooke, and T. Gernon, 2018, Oklahoma's induced seismicity strongly linked to wastewater injection depth: Science, **359**, 1251–1255, doi: 10.1126/science.aap7911.

Hiscott, R. N., 1978, Provenance of Ordovician deep-water sandstones, Tourelle Formation, Quebec, and implications for initiation of the Taconic orogeny: Canadian Journal of Earth Sciences, **15**, 1579–1597, doi: 10.1139/e78-163.

Hornbach, M. J., H. R. DeShon, W. L. Ellsworth, B. W. Stump, C. Hayward, C. Frohlich, H. R. Oldham, J. E. Olson, M. B. Magnani, C. Brokaw, and J. H. Luetgert, 2015, Causal factors for seismicity near Azle, Texas: Nature Communications, **6**, 1–11, doi: 10.1038/ncomms7728.

Hornbach, M. J., M. Jones, M. Scales, H. R. DeShon, M. B. Magnani, C. Frohlich, B. Stump, C. Hayward, and M. Layton, 2016, Ellenburger wastewater injection and seismicity in North Texas: Physics of the Earth and Planetary Interiors, **261**, 54–68, doi: 10.1016/j.pepi.2016.06.012.

Ijirigho, B. T., 1981, Secondary porosity and hydrocarbon production from the Ordovician Ellenburger Group of the Delaware and Val Verde Basins, West Texas: Ph.D. dissertation, University of Arizona.

Kerans, C., 1988, Karst-controlled reservoir heterogeneity in Ellenburger Group carbonates of West Texas: AAPG Bulletin, **72**, 1160–1183.

Kerans, C., 1989, Karst-controlled reservoir heterogeneity and an example from the Ellenburger Group (Lower Ordovician) of West Texas: The University of Texas at Austin, Bureau of Economic Geology, Report of Investigations 186, 40.

Kerans, C., 1990, Depositional systems and karst geology of the Ellenburger Group (Lower Ordovician), subsurface West Texas: The University of Texas at Austin, BEG Report of Investigations 193, 63.

Krause, S. J., 1996, Stratigraphic framework, facies analysis, and depositional history of the Middle to Late Cambrian Riley Formation, Central Texas: Master's thesis, The University of Texas at Austin.

Kupecz, J. A., and L. S. Land, 1991, Late-stage dolomitization of the Lower Ordovician Ellenburger Group, West Texas: Journal of Sedimentary Research, **61**, 551–574, doi: 10.1306/D426775D-2B26-11D7-8648000102C1865D.

Loucks, R. G., 1999, Paleocave carbonate reservoirs: Origins, burial-depth modifications, spatial complexity,

and reservoir implications: AAPG Bulletin, **83**, 1795–1834.
Loucks, R. G., and C. Kerans, 2019, Review of the Lower Ordovician Ellenburger Group of the Permian Basin, West Texas and southeast New Mexico, *in* S. C. Ruppel, ed., Anatomy of a Paleozoic basin: The Permian Basin, USA: AAPG Memoir 124: The University of Texas at Austin, Bureau of Economic Geology Report of Investigations 285.
Lucia, F. J., 1995, Rock-fabric/petrophysical classification of carbonate pore space for reservoir characterization: AAPG Bulletin, **79**, 1275–3000.
McBride, E. F., A. A. Abdel-Wahab, and K. L. Milliken, 2002, Petrography and diagenesis of a half-billion-year-old cratonic sandstone (Hickory), Llano region, Texas: The University of Texas at Austin, Bureau of Economic Geology, Report of Investigations 264, 77.
Montgomery, S. L., D. M. Jarvie, K. A. Bowker, and R. M. Pollastro, 2005, Mississippian Barnett Shale, Fort Worth basin, North-Central Texas: Gas-shale play with multi-trillion cubic foot potential: AAPG Bulletin, **89**, 155–175, doi: 10.1306/09170404042.
National Research Council, 2013, Induced seismicity potential in energy technologies: National Academies Press, 262.
Olorunsola, O., F. Li, O. Aboaba, G. R. Keller, and K. J. Marfurt, 2015, An integrated geophysical approach to understanding the structure and the evolution of the Ouachita Orogenic Belt, Fort Worth Basin, Texas: 85th Annual International Meeting, SEG, Expanded Abstracts, 1587–1591, doi: 10.1190/segam2015-5930971.1.
Pettigrew, R. J., Jr., 1991, Geology and flow systems of the Hickory aquifer, San Saba County, Texas: Baylor Geological Studies Bulletin, **51**, 54.
Quinones, L. A., H. R. DeShon, S.-J. Jeong, P. Ogwari, M. M. Scales, and K. B. Kwong, 2019, Tracking induced earthquakes in the Fort Worth Basin: A summary of the 2008-2018 North Texas earthquake study catalog: Bulletin of the Seismological Society of America, **109**, 1203–1216.
Railroad Commission of Texas, 2016, http://www.rrc.texas.gov/about-us/resource-center/research/online-research-queries/, accessed 1 November 2016.
Ross, R. J., 1976, Ordovician sedimentation in the western United States, *in* M. G. Bassett, ed., The Ordovician system: Proceedings of a Paleontological Association Symposium, 73–105.
Scales, M. M., H. R. DeShon, M. B. Magnani, J. I. Walter, L. Quinones, T. L. Pratt, and M. J. Hornbach, 2017, A decade of induced slip on the causative fault of the 2015 M_w 4.0 Venus earthquake, Northeast Johnson County, Texas: Journal of Geophysical Research: Solid Earth, **122**, 7879–7894, doi: 10.1002/2017JB014460.
Shah, A. K., and G. R. Keller, 2017, Geologic influence on induced seismicity: Constraints from potential field data in Oklahoma: Geophysical Research Letters, **44**, 152–161, doi: 10.1002/2016GL071808.
Sloss, L. L., 1976, Areas and volumes of cratonic sediments, western North America and eastern Europe: Geology, **4**, 272–276, doi: 10.1130/0091-7613(1976)4<272:AAVOCS>2.0.CO;2.
Sullivan, E. C., K. J. Marfurt, A. Lacazette, and M. Ammerman, 2006, Application of new seismic attributes to collapse chimneys in the Fort Worth Basin: Geophysics, **71**, no. 4, B111–B119, doi: 10.1190/1.2216189.
Turner, G. L., 1957, Paleozoic stratigraphy of the Fort Worth Basin, *in* F. B. Conselman, ed., Joint field trip guidebook: Abilene Geological Society and Fort Worth Geological Society, 57–78.
United States Geological Survey (USGS), 2018, Earthquake catalog, https://earthquake.usgs.gov/earthquakes/search/, accessed 15 October 2018.
USGS Digital Elevation Model, 2017, 1/3rd arc-second digital elevation models (DEMs) — USGS National Map 3DEP downloadable data collection, https://catalog.data.gov/harvest/object/d71417b1-5d06-4ecb-ab04-196adfc3bd71/html, accessed 10 December 2017.
Walper, J. L., 1977, Paleozoic tectonics of the southern margin of North America: Gulf Coast Association of Geological Societies Transactions, **27**, 230–241.
Walper, J. L., 1982, Plate tectonic evolution of the Fort Worth Basin, *in* C. A. Martin, ed., Petroleum geology of the Fort Worth Basin and Bend Arch area: Dallas Geological Society, 237–251.
Walsh, F. R., and M. D. Zoback, 2015, Oklahoma's recent earthquakes and saltwater disposal: Science Advances, **1**, e1500195, doi: 10.1126/sciadv.1500195.
Watson, W. G., 1980, Paleozoic stratigraphy of the Llano uplift area: A review, *in* D. Windle, ed., Geology of the Llano region, Central Texas: Guidebook to the annual field trip of the West Texas Geological Society: West Texas Geological Society 73, 28–51.
Wright, W. F., 1962, The Ellenburger as a habitat of Permian basin oil: Oil and Gas Journal, **60**, 140–144.
Wright, W. F., 1979, Ellenburger, *in* W. F. Wright, ed., Petroleum geology of the Permian basin: West Texas Geological Society Publication, 13–20.
Zhang, Y., M. Person, J. Rupp, K. Ellett, M. A. Celia, C. W. Gable, B. Bowen, J. Evans, K. Bandilla, P. Mozley, T. Dewars, and T. Elliot, 2013, Hydrogeologic controls on induced seismicity in crystalline basement rocks due to fluid injection into basal reservoirs: Groundwater, **51**, 525–538, doi: 10.1111/gwat.12071.

Katie M. Smye received a B.Sc. in geology from the University of Oklahoma and a Ph.D. from the University of Cambridge. She is a geologist at the Bureau of Economic Geology, University of Texas at Austin. Her research interests include geologic and petrophysical analysis of shale gas and oil plays, and characterization of intervals utilized for disposal of flowback and produced water.

Casee R. Lemons is the director of geoscience at Sourcewater Inc. in Houston, Texas. She was the principal

investigator for this research project for the TexNet-CISR research collaborative at the Texas Bureau of Economic Geology. Her expertise is in integrated geological studies in the oil and gas industry.

Raymond L. Eastwood received a B.S. in physics and an M.S. in geology from Kansas State University and a Ph.D. in geology from the University of Arizona. He is a research fellow at the Bureau of Economic Geology, Jackson School of Geosciences, University of Texas at Austin. He worked for ARCO at the Plano Research Center, Plano, Texas, for 18 years in geologic, geophysical, and engineering research as a petrophysicist and for ARCO Alaska and BP/Alaska for five years before retiring in 2002. He was an assistant professor of geology at Northern Arizona University from 1970 to 1979, when he joined ARCO.

Guinevere McDaid received a B.Sc. in geography and anthropology as well as a M.S. in geography from Texas State University San Marcos. She is an energy data and GIS analyst at the Bureau of Economic Geology, University of Texas at Austin. Her expertise is in geodatabase creation and management, geospatial data analyses, map design, and data mining.

Peter H. Hennings is a research scientist at The University of Texas Bureau of Economic Geology, where he is principal investigator in the Center for Integrated Seismicity Research and a lecturer in the Department of Geological Sciences. He worked in the petroleum industry for 25 years as a research scientist (Mobil Oil and Phillips Petroleum) and technical manager (ConocoPhillips).